Three-dimensional time resolved fluid mechanics simulation of an EWOD-driven micropump

S. Bohm[1,2], L. Dittrich[2], E. Runge[1]
[1]Group "Theoretical Physics I", Technische Universität Ilmenau, Ilmenau, Germany
[2]5microns GmbH, Ilmenau, Germany

Abstract
Due to the advantageous scaling upon miniaturisation, the so-called electrowetting-on-dielectrics effect (short EWOD-effect) is suitable for the manipulation of liquids on the micro or nanoscale. This article shows how an EWOD-driven micropump can be simulated in COMSOL Multiphysics®. The theoretical description as well as the developed simulation methods are presented and discussed. In addition, numerical results are shown, and the influence of important system parameters is investigated. Finally, design rules for a nearly optimal pump design are derived.

Introduction

This work reports how a novel EWOD-driven micropump is simulated using COMSOL Multiphysics® [1]. Electrowetting-on-Dielectrics (EWOD) is a frequently used technique to manipulate liquids on small scales. With the help of the EWOD-effect and the use of topological optimized Tesla-valves, a pump can be manufactured that does not require any moving components [2,3]. The pump chamber made of silicon contains a few hundred thousand of deep-etched cavities (see Fig. 1). A hydrophobic layer is applied on top of an intermediate dielectric layer on the surface of the cavities to force the liquid into the Cassie-Baxter state [4]. By applying an alternating voltage between the liquid and the heavily doped silicon, the wetting properties of the liquid change, and the liquid-vapor interface is periodically and reversibly deflected inside the microcavities. The goal of the simulation is to determine the frequency-dependent flow rate of the micropump.

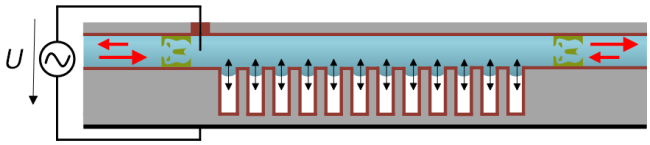

Figure 1. Schematic view of the novel EWOD-driven micropump; dark red areas show isolating dielectric layers; green areas show passive valves

To achieve the objective, an analytical model for the deflection of the liquid-vapor interface inside the microcavities is used and combined with a time-dependent three-dimensional flow simulation using the COMSOL CFD-Module. The fluidic properties of the micropump, like the maximum pump pressure or the flowrate, can be tailored by varying the geometry of the cavities, the type and thickness of the dielectric intermediate layer or the hydrophobic coating. Simulation results for different sets of parameters are presented and discussed.

Theory

EWOD fundamentals

The pump mechanism of the novel micropump is based on the EWOD-effect. The theoretical framework for the description of the EWOD-effect was laid by GABRIEL LIPPMANN in 1875 [5]. He found that the interfacial tension between a solid and a liquid γ_{sl} depends on the electrical surface charge density ϱ_{sl}:

$$\left.\frac{\partial \gamma_{\mathrm{sl}}}{\partial U}\right|_{T,\mu=\mathrm{konst.}} = -\varrho_{\mathrm{sl}} \qquad (1)$$

where U describes the voltage difference across the interface. The standard experimental set-up for investigating the EWOD-effect is shown in Fig. 2, namely the contact angle measurement on sessile droplets on top of a hydrophobic dielectric layer.

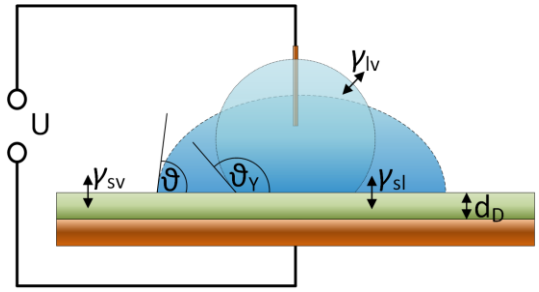

Figure 2. Classical EWOD-experiment; an electrical voltage difference across the interface leads to a decrease of the contact angle at the triple phase contact line

Under the simplifying assumption that the system in Fig. 2 can be described as a plate capacitor carrying the surface charge density $\rho_{\mathrm{sl}} = (\varepsilon_0\, \varepsilon_{\mathrm{r,D}}\, U)/d_{\mathrm{D}}$ where d_{D} is the thickness of dielectric interface and $\varepsilon_{\mathrm{r,D}}$ its permittivity, equation (1) can be analytically integrated. This leads to:

$$\gamma_{\mathrm{sl}}(U) = \gamma_{\mathrm{sl,0}} - \frac{\varepsilon_0 \varepsilon_{\mathrm{r,D}}}{2 d_{\mathrm{D}}} U^2 \qquad (2)$$

Insertion into the well-known Young equation:

$$\cos\vartheta_{\mathrm{Y}} = \frac{\gamma_{\mathrm{sv}} - \gamma_{\mathrm{sl}}(U)}{\gamma_{\mathrm{lv}}} \qquad (3)$$

yields an expression for the voltage-dependent contact angle $\vartheta(U)$ at the triple-phase contact line:

$$\cos\vartheta(U) = \cos\vartheta_{\mathrm{Y}} + \frac{\varepsilon_0 \varepsilon_{\mathrm{r,D}}}{2 d_{\mathrm{D}} \gamma_{\mathrm{lv}}} U^2 \qquad (4)$$

Analytical model of the multiphase flow inside a single microcavity

Theoretically, the flow within the microcavities can be described using a multiphase flow simulation, whereby the compressibility of the enclosed gas and the voltage-dependent wetting properties must be considered. However, due to the high number of microcavities, the calculation effort would be far too high. Therefore, an analytical model for the description of the multiphase flow inside a single microcavity is combined with a three-dimensional time-dependent single-phase fluid

flow simulation. Thus, the microcavities do not need to be explicitly modelled. The analytical model for the description of the EWOD-driven flow inside of a single microcavity is based on the model of MATSUMOTO and COLGATE [6]. From the analytical model a voltage and volume-dependent pressure response function of a single cavity is determined and used as the inlet boundary condition for the fluid flow simulation. The voltage difference across the dielectric interface of each microcavity leads to a decrease of the contact angle according to equation (4). The decrease of the contact angle is linked to a decrease of the interface curvature and as a result to a change of the Laplace-pressure. The introduced pressure gradient initiates a flow and the interface moves into the microcavity. The gas inside the cavity is compressed by the movement of the interface. The movement of the interface stops when the Laplace-pressure p_L is equal to the difference of the gas pressure $\mathrm{p_G}$ of the enclosed gas minus the potentially applied overpressure p_0 at the outlet of the micropump. Therefor the equilibrium condition is:

$$p_L = p_\mathrm{G} - p_0 \tag{5}$$

Under the assumption that we can describe the enclosed gas as an ideal gas, the pressure is linked to the interface deflection by:

$$p_\mathrm{G}\big(l_0(U)\big) = \frac{L}{L - l_0(U)} p_\mathrm{at} \tag{6}$$

where p_at denotes the pressure of the empty cavity, L is the overall length of a microcavity and $l_0(U)$ describes the voltage-dependent equilibrium position of the interface.
The voltage-dependent Laplace-pressure for a cylindrical shaped microcavity is obtained as:

$$p_\mathrm{L}(U) = \frac{2\gamma_\mathrm{lv}\cos\vartheta(U)}{R} \tag{7}$$

The insertion of equation (6) and (7) into the equilibrium condition (5) leads to an equation for the voltage-dependent equilibrium position of the interface:

$$l_0(U) = L\left(1 - \frac{p_\mathrm{at}}{p_0 + \frac{2\gamma_\mathrm{lv}\cos\vartheta(U)}{R}}\right) \tag{8}$$

The voltage-dependent contact angle $\vartheta(U)$ is calculated by equation (4). The function $l_0(U)$ is shown in Fig. 3 for different values of the length L of the cavity. The strong non-linear dependence on the contact angle becomes visible. A larger value of the etch depth L leads to an increase of the maximum possible deflection of the interface inside each microcavity.

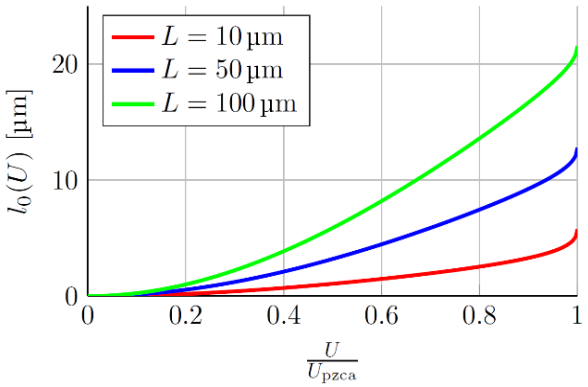

Figure 3. Voltage-dependent equilibrium position $l_0(U)$ for different etch depths L of the microcavities; the applied voltage is normalized by the voltage which is necessary for a vanishing contact angle according to equation (4)

So far, all equations have been derived for the stationary case. In order to be able to use the equations also for a time-dependent description of the interface movement, the following assumptions are made:

1. The inertia of the liquid within a microcavity is negligible compared to the overall inertia of the liquid inside the pump chamber. The deflection of the interface is regarded as quasi-static and is assumed to follow the external applied voltage instantaneously.
2. The deformation of the interface happens instantaneously.
3. The introduced pressure difference according to equation (7) is independent of the vertical position of the interface inside the cavity and is solely determined by the applied voltage difference U.

Under these assumptions and the realization that equation (6) still holds for arbitrary values of the deflection l_0 the overall voltage and deflection-dependent pressure difference at the inlet of the cavity can be calculated as:

$$p_\mathrm{in}\big(l(t), U(t)\big) = p_{\mathrm{L},0} - p_\mathrm{L}\big(U(t)\big) + p_\mathrm{G}\big(l(t)\big) - p_0 \tag{9}$$

where $p_{\mathrm{L},0}$ denotes the Laplace pressure at zero voltage. Equation (9) shows that the total driving pressure of a microcavity is a function of the time-dependent interface position and the time-dependent applied voltage. Additionally, the interface position is linked to the net pumped volume of the fluid. The actual position of the interface can be determined by:

$$l(t) = L\left(l_o(U=0) - \frac{V_\mathrm{res}(t)}{N \cdot A}\right) \tag{10}$$

if the net pumped volume V_res, the number of cavities N and the cross-sectional area A of each cavity are known. The net pumped volume is associated to the actual velocity field at the two outlets of the geometry via:

$$V_\mathrm{res}(t) = \int_0^t \left(\int \boldsymbol{u}(\boldsymbol{t}) \cdot \boldsymbol{n}\mathrm{d}A_1 + \int \boldsymbol{u}(\boldsymbol{t}) \cdot \boldsymbol{n}\mathrm{d}A_2\right)\mathrm{d}t \tag{11}$$

where $\boldsymbol{n}$ is the outward pointing normal at the outlet. Thus, the strong coupling between the velocity field $\boldsymbol{u}(t)$ and the inlet pressure p_in becomes clear. The inlet pressure determines the velocity field and at the same time the inlet pressure is determined by the velocity field.
A challenge in using equation (8) for the modelling of the interface movement is that the deflection becomes negative for small voltages or a low value of the overpressure p_0 due to the nonwetting surface of the cavities and the resulting capillary depression. Under normal conditions the applied pressure p_0 is equal to the ambient pressure during the filling of the micropump and therefor p_at is also equal to p_0. For a nonwetting surface the Young contact angle is larger than 90° and thus the value of the interface deflection according to equation (8) would become negative. In this case the interface is assumed to be flat and therefor the Laplace-pressure vanishes. As soon as the applied voltage or the overpressure exceeds a certain threshold the deflection becomes positive and can be calculated with equation (8). To model this behavior correctly the values of $p_\mathrm{L}(U)$ and $l(t)$ are set to zero if they are negative.

Simulation geometry

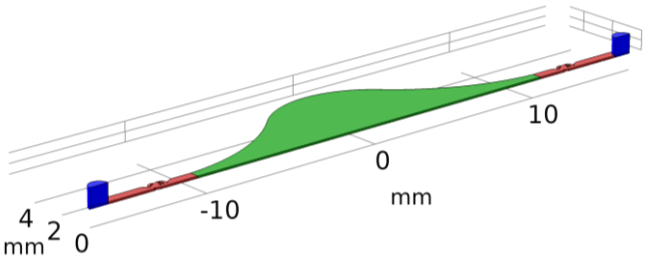

Figure 4. Three-dimensional geometry of the simulated micropump; the green part shows the pump chamber; red parts show the passive Tesla-valves; blue parts show the fluidic connections

For the time-dependent fluid flow simulation, a three-dimensional model of the micropump is created. The geometry of the micropump is mainly generated using the built-in COMSOL functions for the creation and manipulation of geometries. Two two-dimensional drawings of the pump chamber and the topological optimized Tesla-valves are used as input files. The drawings are saved as dxf-files and imported into separated work planes. Afterwards both drawings are extruded defining the etch depth of the pump chamber. The resulting domains of the Tesla-valves are subtracted from the pump chamber domain using a Boolean operation. Two additional cylinders with a height of $1000\ \mu m$ are inserted to model the fluidic connections at both ends of the pump chamber. In the final step one half of the geometry is removed in order to take advantages of the symmetry of the model and as a result reduce the computational effort. An example of the final simulation geometry is shown in Fig. 4.

Tesla-valves

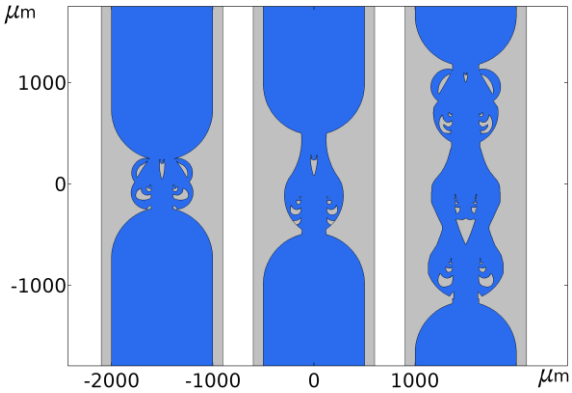

Figure 5. Examples for the geometries of three different topological optimized Tesla-valves; blue areas show the etched areas

In order to be able to manufacture a micropump that does not require any moving components at all, passive valves must be used for the rectification of the pump stroke. The basic principle of passive valves is that the fluidic resistance differs strongly for the two opposite flow directions. A measure for the quality of a passive valve is the ratio of the pressure drop (at a constant flow rate) or the ratio of the flowrates (at a constant pressure difference) for the different flow directions. This ratio is called the diodicity and it should be as large as possible. Because the diodicity is always finite, the flow cannot be completely blocked and no constant pressure difference can be built up, which are the main challenges in using passive vales in fluidic systems. The diodicity strongly depends on the geometry of the valve and the flow rate but is also influenced by the properties of the fluid like the viscosity and the density. A particularly efficient type of passive valve is called a Tesla-valve in honor of its inventor NICOLA TESLA [7].

To find a nearly optimal geometry of the Tesla-valves, a topological optimization is carried out. Details about the basic principles of the topological optimization can be found in [8]. A basic example for the implementation of a topological optimization of a Tesla-valve in COMSOL can be found in the application library (Application ID: 14513). The topological optimization directly delivers the material distribution within the user specified spatial area. This material distribution is translated into a two-dimensional drawing and afterwards can be directly used as an input for the fluid flow simulation. Three different examples for the resulting geometries of the Tesla-valves are shown in Fig. 5.

Numerical Model

The simulation model is based on the Navier-Stokes equations. A *Laminar Flow* interface is used for the simulation. The fluid is assumed to be incompressible. The governing equations are:

$$\varrho \frac{\partial \boldsymbol{u}}{\partial t} + \varrho(\boldsymbol{u} \cdot \boldsymbol{\nabla})\boldsymbol{u} = \boldsymbol{\nabla} \cdot [\mu(\nabla \mathbf{u} + (\nabla \mathbf{u})^{\mathrm{T}}) - p\boldsymbol{I}] \qquad (12)$$

$$\nabla \boldsymbol{u} = 0 \qquad (13)$$

Here ϱ denotes the density and μ describes the dynamic viscosity of the fluid. An outlet boundary condition is set on the top faces of each cylinder with a prescribed pressure of zero pascal. The *suppress backflow* option is deselected to allow a flow in both directions across the outlet boundaries. A symmetry condition is applied to all faces in the middle plane of the geometry. An inlet boundary condition with a prescribed pressure is set on the back of the pump chamber in the area where the cavities would be located. The inlet pressure $p_{\mathrm{in}}\big(l_0(t), U(t)\big)$ is calculated using equation (9). To ensure that the limited volume stroke of the cavities is modelled correctly, the pressure difference on the inlet is linked to the overall volume difference at the two outlets of the micropump via two additional global differential equations. These two equations are formulated as follows:

$$0 = \frac{\partial V_{1/2}}{\partial t} - \int \boldsymbol{u}(\boldsymbol{t}) \cdot \boldsymbol{n} \mathrm{d}A_{1/2} \qquad (14)$$

The initial values are chosen as $V_{1/2}(t = 0) = 0$. For the evaluation of the integrals two integral operators are introduced. With the help of equation (14) the net pumped volume can be calculated via:

$$V_{\mathrm{res}}(t) = 2 \cdot \big(V_1(t) + V_2(t)\big) \qquad (15)$$

The pre-factor is required because half of the geometry has been removed to take advantage of the symmetry of the geometry. Theoretically the time-dependent function $U(t)$ can be arbitrarily chosen. To determine the frequency-dependent volume flow rate, it seems natural to use a harmonic time dependence $U(t) = U_0 \sin(2\pi f t)$ and to vary the frequency. In this case the system should be simulated for at least five periods for each frequency value to exclude the transient initial phase. Instead, to keep the simulation time short and the amount of data small, we use a chirped voltage signal of the form:

$$U(t) = U_0 \sin(\pi k t \cdot t) \qquad (16)$$

to excite the micropump: The frequency is increased linearly from 0 to 400 Hz over a period of six seconds leading to a value of $k = \frac{400}{6}\frac{Hz}{s}$. Thus, the frequency-dependent flow rate can be determined from a single simulation. To reduce the spectral ripples and to make the transitions at the start and the end of the chirp less sudden, linear rise and fall times with a duration of 0.1 s are introduced. A sampling rate of $f_S = 8192$ Hz is used for the generation of the chirp resulting in a time step of $\Delta t = 1/f_s$ seconds. The power density spectrum of the chirp is shown in Fig. 6. The chirp signal is saved as a text file and imported in COMSOL as an *interpolation function*. Otherwise an *analytical function* could be introduced.

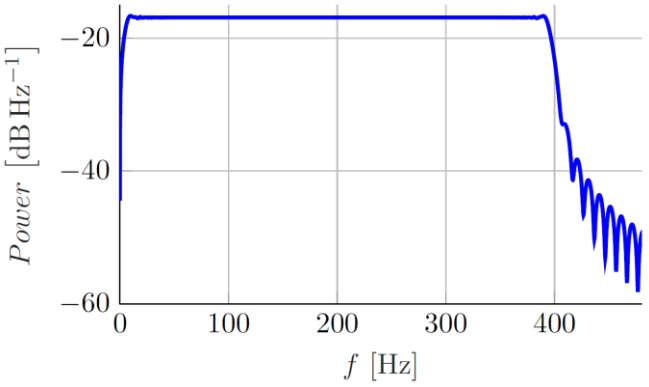

Figure 6. Power spectral density of the chirp signal; As desired, an almost constant amplitude spectrum is obtained.

For the fluid flow simulation, the time step is fixed to the value of Δt and the *consistent initialization* option is turned off. Therefore, for each simulation, 49152 time steps have to be calculated. To keep the amount of data manageable, the velocity and pressure fields are not stored in the output. During the simulation the time-dependent parameters $l_0, p_{\text{in}}, V_1, V_2, \dot{V}_1, \dot{V}_2$ and V_{res} are evaluated using *global probes* and accumulated in a single *probe table*. The results are exported, and the final evaluation is carried out in Matlab [9]. The simulations are done on the Massively Parallel Compute Cluster (MaPaCC) of the Technische Universität Ilmenau. Each simulation is running on two Intel® Xeon® CPU E5-2650 v4 at 2.20 GHz using 2 sockets with 12 cores in total. Depending on the selected parameters, a simulation takes between 72 and 150 hours and requires on average about 6 GB of memory.

Mesh generation

In order to obtain numerically meaningful results with a simultaneously low computing time, the mesh must be created appropriately. The first step is to triangulate the complete backside of the micropump. The maximum element size is fixed to 150 µm and the minimum size is set to 10 µm. Afterwards the *swept* feature is used, and a volume mesh is created by sweeping the mesh from the source faces of the backside along the pump chamber to the opposite destination faces on the top side. In order to map the boundary flows correctly, a *symmetric arithmetic distribution* with an element ratio of 2.5 and seven elements is used for the swept mesh. Afterwards the same is done for the two attached cylinders but for the swept mesh an equidistant distribution with a fixed number of ten elements is used. The final mesh consists of approximately 50.000 elements with an average element quality better than 0.87 whereby the skewness is taken as the quality measure.

Validation of the numerical simulation

To validate the model, a simulation was first carried out in which the voltage was increased linearly. The used parameters are listed in table 1. The time-dependent deflection of the fluid-air interface is shown in Fig. 7. As expected, the deflection below the threshold voltage vanishes and then rises until the maximum value of $l_0(U = 100\ V) = 14.68$ µm is reached and the interface movement stops. Additionally, the time-dependent pressure $p_{\text{in}}(t)$ has been investigated. It is shown in Fig. 8. Until the threshold voltage is reached the pressure vanishes as expected. After that, the pressure initially increases very quickly because the liquid needs a certain time to start moving because of its inertia. During this time the voltage further increases leading to a pressure difference of approximately 20 Pa. After less than one millisecond, the liquid within the pump chamber moves at an almost constant speed and the inlet pressure stays also nearly constant. However, the non-linear dependence of the interface deflection on the applied voltage becomes visible again.

Table 1: Parameters used unless otherwise specified

Parameters	Values
Radius R	5.64 µm
Etch depth L	80 µm
Number of cavities N	250000
Surface tension γ_{lv}	0.073 N/m
Density ϱ	1000 kg/m^3
Viscosity μ	0.001 Pa · s
Young angle ϑ_{Y}	100°
Thickness dielectric layer d_{D}	2.1 µm
Permittivity ε_{r}	3.7
Voltage amplitude U_0	100 V
Etch depth pump chamber	100 µm

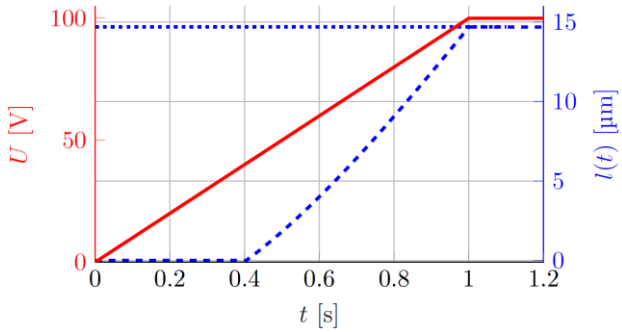

Figure 7. Validation of the simulation model; solid red line shows the time-dependent voltage; dashed blue line shows the time-dependent interface deflection; dotted blue line shows the equilibrium position according to equation (8)

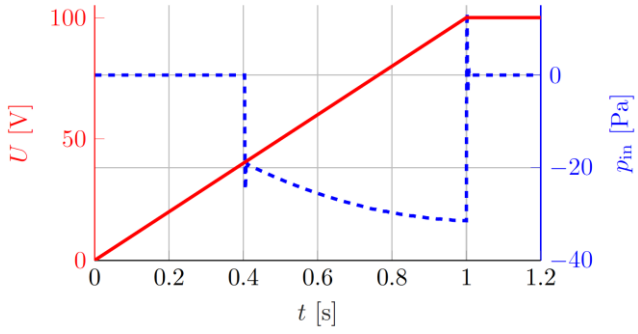

Figure 8. Validation of the simulation model; solid red line shows the time-dependent voltage; dashed blue line shows the time-dependent inlet pressure p_{in} according to equation (9)

Simulation results

After the simulation is finished, the table with all relevant results is exported and further processed in Matlab. An example for the simulated curve of the deflection $l(t)$ of the interface is shown in Fig. 9. At small frequencies the deflection oscillates between zero and a positive value and can even exceed the maximum value of $l_0(U_0)$ due to the inertia of the liquid. At high frequencies the interface position oscillates around a non-zero equilibrium position. The amplitude of the deflection decreases with increasing frequency due to the inertia of the liquid.

For the determination of the frequency-dependent flow rate the spectrogram of the difference of the time-dependent flow rates at the two outlets is calculated. The spectrogram is calculated using a Short-Time Fourier Transform (STFT). A Hann-window with a width of 2048 samples, an overlap of 1850 samples and a sample rate of 8192 Hz is used for the calculation. An example for the spectrogram of the flow rate at a single outlet is shown in Fig. 10. Because of the nonlinear dependence of the contact angle on the applied voltage, special care must be taken, and the system cannot be analyzed with the conventional methods of linear system analysis. However, for a frequency that increases slowly with time the spectrogram shows almost exclusively a DC-component and a component with twice the current frequency. However, the double-frequency components and possible higher harmonics cancel each other out when the difference of the flow rates is calculated and mainly a DC-component remains. This becomes clear when we look at the function $V_{\mathrm{res}}(t)$ shown in Fig. 11, which shows only very small oscillations.

Parametric studies

The response of the system is determined by a large number of parameters. Therefore, a complete parameter analysis cannot be performed. However, the influence of certain system parameters can be investigated and general design guidelines for an optimal pump design can be derived.

For all simulations, the parameters from table 1 were used unless otherwise stated. The geometry which is used for the simulation is shown in Fig. 4. In Fig. 12 the influence of the etch depth of a single cavity on the frequency-dependent flow rate is shown. The maximum flow rate decreases with a decreasing etch depth. This can be understood by means of a mechanical equivalent circuit diagram. The enclosed vapor acts as a spring and generates the restoring force for fluid. For a decreasing etch depth, this spring becomes more and more stiff leading to a decrease of the deflection of the fluid-air interface and therefore to a decreased volume stroke but at the same time the maximum of the flow rate is shifted to higher frequencies. From an electrical point of view, the micropump represents a capacitive load. This makes the driving of the pump increasingly difficult as the frequency increases. At the same time, however, the fabrication of the shorter microcavities is simpler and less expensive due to the lower aspect ratios and the reduced etch time. Thus, the choice of a suitable length is a tradeoff between the manufacturing and the actuation effort. In Fig. 13, the dependence of the flow rate on the amplitude of the driving voltage is shown. The maximum flow rate decreases as expected with a decreasing amplitude. For high amplitudes of the driving voltages, the quadratic dependence of the contact angle on the voltage amplitude (see eq. (4)) becomes visible if

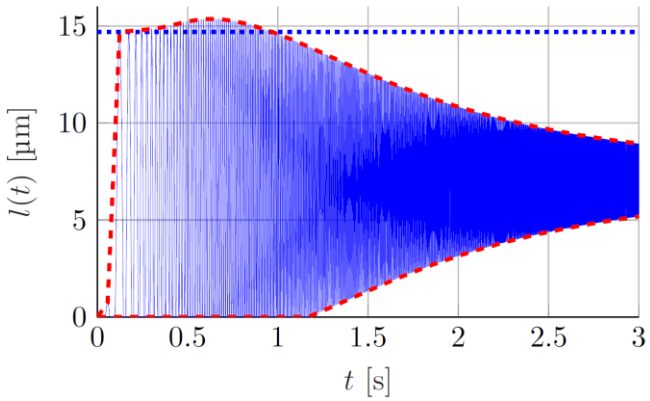

Figure 9. Example of the time-dependent function $l(t)$ plotted as thin solid blue line; dashed red lines indicate the envelope of the deflection curve; dotted blue line shows the equilibrium position according to equation (8)

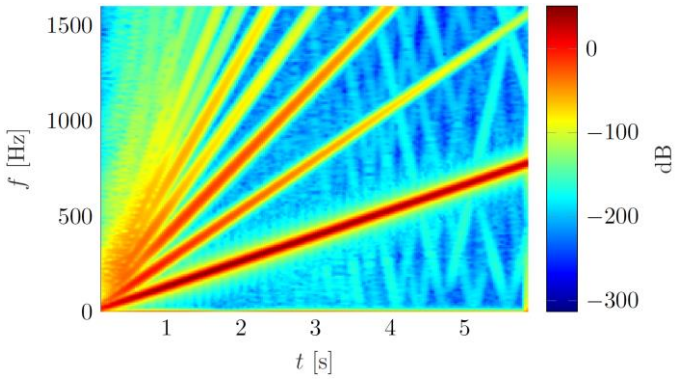

Figure 10. Spectrogram of the time-dependent flow rate $\dot{V}_1$

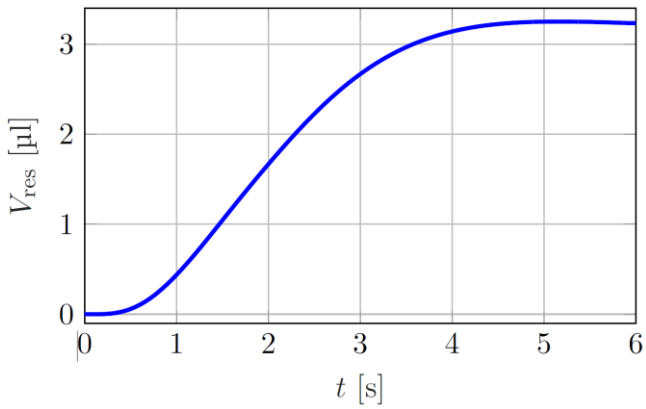

Figure 11. Example of the simulated net pumped volume V_{res}

the non-linear dependence of the interface deflection according to equation (8) is considered. The ratios of the maximum deflections according to equation (8) for the chosen parameters are: $\frac{l(U=100\,V)}{l(U=75\,V)} = 1.89$, $\frac{l(U=100\,V)}{l(U=60\,V)} = 3.65$ which are also approximately reflected in the ratios of maximum flow rates. However, for a voltage only slightly above the threshold voltage of 40.3 V, an almost disappearing volume flow is shown due to the low inlet pressure and the resulting low average velocity. At such low velocities the Tesla-valves are very inefficient, and the rectifying action vanish.

Finally, the dependence of the flow rate on the number of microcavities is shown in Fig. 14. We see that the maximum flow rate decreases as expected with a decreasing number of microcavities but there is only a weak dependence for a high

number of cavities. In this parameter regime the flow rate is limited by the finite diodicity of the Tesla-valves and not by the limited deflection of the fluid-air interface inside each microcavity. Even if the volume stroke increases with a higher number of cavities, the resulting net volume flow need not necessarily increase due to the limited diodicity. This implies that for further optimization, the system size could be reduced by reducing the number of cavities while maintaining almost a constant efficiency. However, for a very small number of cavities, the flow rate vanishes due to the limited volume stroke.

Summary and conclusions

We presented how an EWOD-driven micropump can be efficiently simulated using COMSOL Multiphysics®. The strong coupling between the interface movement and the applied pressure at the inlet could be correctly reproduced in the simulation by adding two additional global equations. By using a chirped signal for the excitation of the micropump the frequency-dependent flow rate can be obtained over a whole range of frequencies within a single simulation. With the help of numerical simulations, the influence of various system parameters has been investigated. The influence of three important design parameters, namely the etch depth L, the number of cavities N and the voltage amplitude U_0 were discussed. In the future, the experimental investigation of micropumps and thus the direct comparison with the simulated curves for the frequency-dependent flow rate for different parameters is planned. Possibilities for technical realization of an EWOD-driven micropump are discussed in reference [3]. Additionally, the multiphase flow model for the single cavity could be improved by the detailed modelling of the voltage-dependent deformation of the interface. An efficient way to do this is presented in [10,11].

Acknowledgement

We thank the Federal Ministry of Economics and Energy for the funding of the research project within the framework of the Zentrales Innovationsprogramm Mittelstand (ZIM, funding number: ZF4457306PO9).

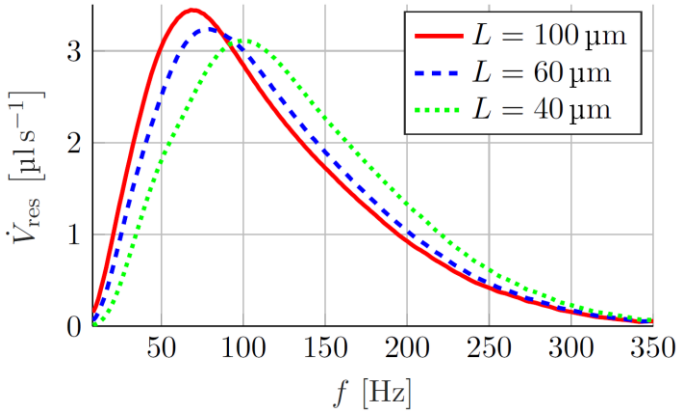

Figure 12. Dependence of the frequency-dependent flowrate $\dot{V}_{res}$ on the etch depth L of the microcavities at $U_0 = 100\,V$

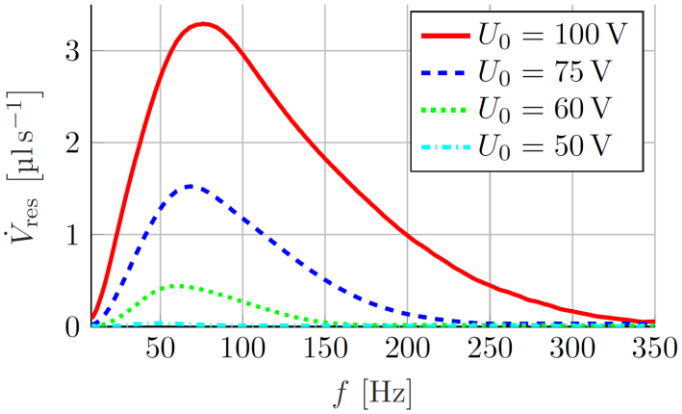

Figure 13. Dependence of the frequency-dependent flowrate $\dot{V}_{res}$ on the amplitude U_0 of the applied voltage curve $U(t) = U_0 \sin(\pi k t \cdot t)$

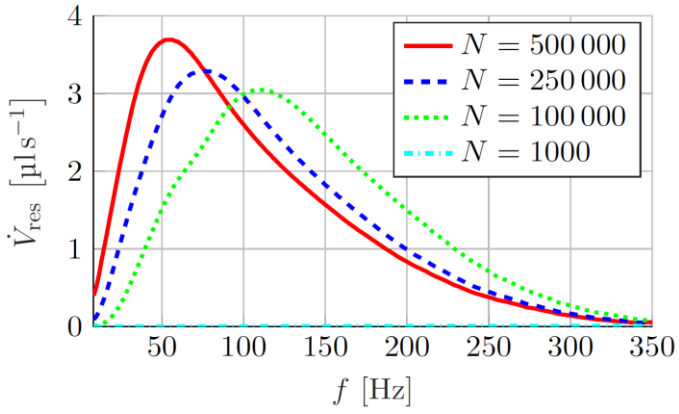

Figure 14. Dependence of the frequency-dependent flowrate $\dot{V}_{res}$ on the total number N of microcavities at $U_0 = 100$

References

1. COMSOL Multiphysics® v.5.4, COMSOL AB, Stockholm, Sweden (2018)
2. Hoffmann, M., Dittrich, L., Bertko, M., Mikropumpe zur Erzeugung einer Fluidströmung, Pumpensystem und Mikro-kanalsystem, WO 2012/084707 A1 (2012)
3. Bohm, S. Dittrich, L., Runge, E., Modellierung, Fertigung und Erprobung einer neuartigen EWOD-betriebenen Mikropumpe, MST-Kongress, Berlin, Germany (2019)
4. Cassie, A. B. D., Baxter, S., Wettability of porous surfaces, *T. Faraday Soc.*, **(40)**, 546-551 (1944)
5. Mugele, F., Baret, J.-C., Electrowetting. From basics to applications, *J. Phys. Condens. Matter*, **(28)**, R705 (2005)
6. Matsumoto, H., Colgate, J., Preliminary investigation of micropumping based on electrical control of interfacial tension, IEEE Proceedings on Micro Electro Mechanical Systems, An Investigation of Micro Structures, Sensors, Actuators, Machines and Robots, Napa Valley, USA (1990)
7. Tesla, N., Circuit elements having no moving parts, USA 1329559A (1920)
8. Lin, S., Zhao, L., Guest, J.K., Weihs, T.P., Liu, Z., Topology Optimization of Fixed-Geometry Fluid Diodes, *J. Mech. Des*, **137-(8)**, 081402-081410 (2015)
9. MATLAB, The MathWorks Inc., Natick, USA, (2018)
10. Bohm, S., Runge, E., Determination of the shape of static liquid/liquid or liquid/vapor interfaces in electrical fields – Theory, simulation and experiments, EPFDC, Ilmenau, Germany (2019)
11. Bohm, S., Runge, E., Fast calculation method for determining the shape of static liquid/liquid or liquid/vapor interfaces under the influence of electrical fields, DPG-Frühjahrstagung der Sektion Kondensierte Materie (SKM), Regensburg, Germany (2019)